Dual Circularly Polarized 3-D Printed Broadband Dielectric Reflectarray With a Linearly Polarized Feed

Qiao Cheng, Yang Hao, *Fellow, IEEE*, Jack McGhee, William G. Whittow, *Senior Member, IEEE*, J. C. Vardaxoglou, *Fellow, IEEE*, Raj Mittra, *Life Fellow, IEEE*, and Shiyu Zhang

***Abstract*— A broadband dual circularly polarized (dual-CP) reflectarray based on 3-D printed dielectric materials is proposed in this article. A novel 3-D dielectric array element that enables the broadband linearly polarization (LP) to CP transformation is proposed. The unit cell consists of two orthogonal dielectric cuboids that adjust the phases of the two orthogonal LP waves independently and then combine them into a CP wave. The innovative unit cell design provides an extra degree of freedom in varying the geometries of the array elements in all three dimensions, which enables us to independently control the phases of the two LP waves. This maintains an equal amplitude and 90° phase difference condition across the entire reflectarray surface, realizing a broadband and high gain LP–CP reflectarray. The placement of the feed is also optimized to achieve the highest aperture efficiency. Finally, an off-set reflectarray was designed and fabricated using lost-cost 3-D printing. The reflectarray is able to provide both left-hand circular polarization (LHCP) and right-hand circular polarization (RHCP), with just an LP feed. The measurements agree well with simulated results where the maximum realized gain and directivity at 34 GHz are measured as 27.9 and 28.1 dBi, respectively. The measured 3 dB gain bandwidth and aperture efficiency are 30% and up to 38%, respectively. More importantly, a broad 3 dB axial ratio (AR) bandwidth greater than 40% has been achieved for both LHCP and RHCP, covering almost the entire frequency band of interest, ranging from 26 to 40 GHz.**

Manuscript received 2 April 2021; revised 16 December 2021; accepted 2 January 2022. Date of publication 20 January 2022; date of current version 26 July 2022. This work was supported by the Engineering and Physical Sciences Research Council (EPSRC) through "SYnthesizing 3-D METAmaterials for RF, microwave and THz applications (SYMETA)" under Grant EP/N010493/1. *(Corresponding author: Shiyu Zhang.)*

Qiao Cheng was with the School of Electronic Engineering and Computer Science, Queen Mary University of London, London E1 4NS, U.K. He is now with the Department of Electrical and Electronic Engineering, The University of Manchester, Manchester M13 9PL, U.K. (e-mail: qiao.cheng@manchester.ac.uk).

Yang Hao is with the School of Electronic Engineering and Computer Science, Queen Mary University of London, London E1 4NS, U.K. (e-mail: y.hao@qmul.ac.uk).

Jack McGhee was with the Wolfson School of Mechanical, Electrical and Manufacturing Engineering, Loughborough University, Loughborough LE11 3TU, U.K. He is now with the Department of Chemistry and the National Graphene Institute, The University of Manchester, Manchester M13 9PL, U.K. (e-mail: jack.mcghee@manchester.ac.uk).

William G. Whittow, J. C. Vardaxoglou, and Shiyu Zhang are with the Wolfson School of Mechanical, Electrical and Manufacturing Engineering, Loughborough University, Loughborough LE11 3TU, U.K. (e-mail: w.g.whittow@lboro.ac.uk; j.c.vardaxoglou@lboro.ac.uk; s.zhang@lboro.ac.uk).

Raj Mittra is with the Department of Electrical and Computer Engineering, University of Central Florida, Orlando, FL 32816 USA, and also with the Department of Electrical and Computer Engineering, King Abdulaziz University, Jeddah 21589, Saudi Arabia (e-mail: rajmittra@ieee.org).

Color versions of one or more figures in this article are available at https://doi.org/10.1109/TAP.2022.3142735.

Digital Object Identifier 10.1109/TAP.2022.3142735

***Index Terms*— 3-D printing, broadband, circular polarization, dielectric antenna, reflectarray.**

I. Introduction

A REFLECTARRAY antenna consists of a reflecting surface of unit cells and a feeding antenna [1], [2]. The unit cells shift the phases of incoming waves such that the reflected waves add constructively in a desired direction. Reflectarray antennas combine the features of both reflector antennas and phased array antennas. They are compact in size, lightweight, have a high gain, and are capable of beamsteering using simple and low-cost tunable elements [3]. Reflectarrays have been extensively studied in the past few decades. Current research focuses on either improving the performance in terms of large bandwidth [4], [5], high gain [6], [7] and high efficiency [8], or exploring new functionalities, such as dual polarization [9], [10], circular polarization [11], [12], multiband [13], [14], multibeam [15], [16], and dynamic beamsteering [3], [17], [18].

Additive manufacturing (3-D printing) with dielectric materials is a trending technology, which enables fast and low-cost prototyping for electromagnetic devices. This technology has already been applied to many antenna designs, such as dielectric resonator antennas [19]–[21], lens antennas [22]–[25], transmitarrays [26], [27], and reflectarrays [28]–[32]. Dielectric reflectarrays are typically less lossy and more efficient than their microstrip counterparts at high frequencies. With the frequency increased, the array elements based on the microstrip suffer from an increased conductor loss in the metallic resonators and the dielectric loss in the microstrip substrate [28], [33]–[35]. Specifically, in 2014, Nayeri *et al.* [28] demonstrated the first 3-D printed reflectarray operating at 100 GHz, in which the height of the dielectric slab is varied to achieve phase variation up to 360°. This study shows that 3-D printing is a promising low-cost solution for high-gain terahertz antennas. Later, Zhang [29] proposed another 3-D printed reflectarray where discrete dielectric cuboids with varying lengths were used as the array element. A maximum gain of 34 dBi with a 1 dB bandwidth of 10% was achieved in the Ka-band. In 2018, Wu *et al.* [30] presented a wideband high gain dielectric reflectarray working at 220 GHz. Similar to [28], the dielectric height is varied for desired phase response. It was found that the maximum gain and 1 dB gain bandwidth are 31.3 dBi and 20.9%, respectively.

While 3-D printing technology has been successfully applied to linearly polarization (LP) reflectarrays, its

application to a circularly polarized (CP) reflectarray is quite limited. CP antennas are widely used in wireless communication systems, such as satellite communications, global positioning systems (GPS), and radio frequency identification (RFID), as they are less susceptible to environmental interference and possess better immunity to multipath propagation effects [36]. As the demands for high-data-rate communication systems increase, it is highly desirable to have CP antennas with wide bandwidths [37]. CP reflectarrays can be realized by using either CP or LP feeds. The latter has the advantages that it can realize multiple polarizations, including left-hand circular polarization (LHCP), right-hand circular polarization (RHCP), and linear, using the same feed. The LP-LHCP and LP-RHCP are the two types of reflectarrays that we focus on in this article. To date, most existing wideband CP reflectarrays are either based on microstrip or all-metal structures [6], [11], [12], [38]–[40]. The main reason for this is the challenge of fabricating dielectric structures with complex 3-D geometries for polarization control.

An all-dielectric CP reflectarray has been proposed in [31] where a hemiellipsoidal dielectric element was adopted. Although this work was based on the concept of wideband hemiellipsoidal dielectric resonator antenna (DRA) and a simulated 1 dB gain bandwidth of 11.2% was achieved, only 6.7% of 3 dB AR bandwidth was reported. Moreover, the curvature of the hemiellipsoid makes it challenging to fabricate accurately with a tight tolerance, which, in turn, may deteriorate the performance of the reflectarray. More recently, Bin *et al.* [32] presented a CP dielectric reflectarray using a cross-shaped dielectric structure. The size of the unit cell was scaled up and down to achieve the desired phase variation. However, since the ratio of the two perpendicular blocks was fixed and scaled simultaneously, it was impossible to independently tune the phase responses for two polarizations. Therefore, in this design, the phase differences become unstable across different scaling factors, which, in turn, deteriorates the conversion to circular polarization. This issue was even more pronounced in the magnitude curves of the reflection where the largest difference exceeded 10 dB, and as a result, only a 3 dB AR bandwidth of 19.3% was realized. In addition, strong reflection magnitudes were observed in both polarizations, resulting in a maximum aperture efficiency of only 16.5%.

Exploiting the development of additive manufacturing technology and the emergence of high dielectric constant 3-D printable materials, we take a step further in the dielectric-based LP–CP reflectarray concept. In this article, a novel 3-D dielectric array element, which enables a broadband LP–CP transformation, is proposed. The dielectric array element comprises two orthogonal dielectric cuboids to provide two orthogonal LP waves with equal amplitudes, accompanied by a 90° phase difference, enabling us to combine these two LP waves into a CP wave. The innovative tunability in all three dimensions of the array element enables us to independently control the phases of the two orthogonal LP components based on the location of the element and maintain the conditions of equal amplitude and 90° phase difference across the entire reflectarray surface, therefore enabling the realization of a broadband and high gain LP–CP reflectarray. To prove the concept and demonstrate the advantages of the dielectric LP–CP reflectarray, a 3-D printed broadband LP–CP reflectarray that operates in the Ka-band is detailed in this article. The reflectarray is designed to have an offset feed to circumvent the feed blockage problem. Geometric parameters of the dielectric unit cell are thoroughly investigated, and their effects on the phase response and bandwidth are presented to give guidance on how to achieve a wideband unit cell design. The reference phase and the feed distance are also investigated to optimize the broadband performance.

This article is organized as follows. Section II introduces the unit cell and parametric study for wideband design. Section III presents the design and analysis of the proposed CP reflectarray. Simulation and measurement results are demonstrated and compared with existing literature. Finally, conclusions are drawn in Section IV.

II. Unit Cell Design and Analysis

A. LP–CP Transformation Unit Cell Design

The unit cell of the LP–CP reflectarray is designed to control the reflected phase in two orthogonal directions independently. It is well known that a CP wave can be decomposed into two orthogonal LP components where they have equal amplitudes and $\pm 90^\circ$ phase difference. Based on this concept, the whole reflectarray can be designed to provide two orthogonal LP waves with equal amplitudes but $\pm 90^\circ$ phase difference, and the two LP waves are combined to realize a collimated CP wave.

To achieve independent tuning at two polarizations, we use two sets of linearly polarized elements, namely, the x and y elements, to realize the LP to CP transformation. The structure of the proposed unit cell is shown in Fig. 1. The LP–CP transformation of the proposed unit cell is shown in Fig. 1(g). The polarization of the LP feed is 45° oriented with regard to either of the two axes such that the LP incident field E^i_{LP} has two equal amplitude components E^i_x and E^i_y with two equal phase components ϕ^i_x and ϕ^i_y along the x- and y-axes, respectively. The x and y elements of the unit cell are designed to interact with x and y components of the incident field, respectively, and to produce reflected fields (E^r_x, ϕ^r_x) and (E^r_y, ϕ^r_y) along the x- and y-axes, respectively. To produce a CP reflected wave E^r_{CP}, it has $\phi^r_x = \phi^r_y \pm 90^\circ$. For a lossless reflectarray, the amplitudes of the incident field and the reflected field are equal. Then, the geometric parameters of both elements are adjusted to introduce $\pm 90^\circ$ phase difference to form a CP wave. The change in all three dimensions (L, W, and H) of x and y elements tunes the reflected phase but to different extents. Taking the y element as an example, the y element is a dielectric block with the dimension of $L_y \times W_y \times H_y$. The width W_y is considerably smaller than the length L_y such that it is mainly responsible for the reflection of the LP wave in the y-direction. Similarly, an x element with the same width and length is placed perpendicularly to the y element to reflect the x-polarized incident wave. H_y and L_y of y elements can be adjusted to introduce the desired ϕ^r_y, while H_x and L_x are used to tune the ϕ^r_x. For ease of visualization, the y element is placed in the center of the unit cell, while four-quarter x elements are placed on the top and bottom sides with a height of H_x.

The 3-D dielectric array element has two advantages compared with the conventional metallic array elements. First, the 3-D tunability offers an extra degree of freedom in controlling

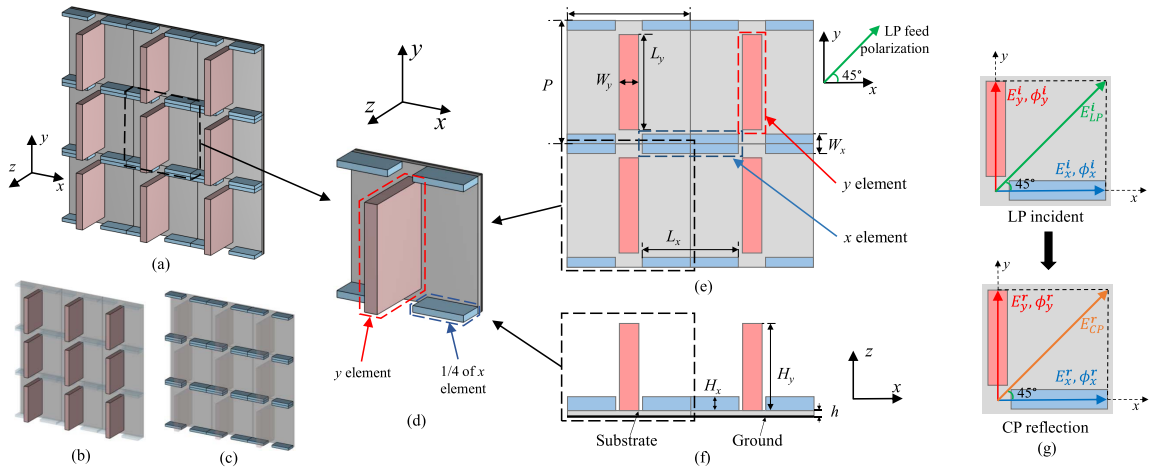

Fig. 1. Geometry of the proposed unit cell. (a) Unit cell in periodic boundary conditions with only (b) y elements visible and (c) x elements visible. (d) Unit cell and its (e) top view, (f) side view, and (g) demonstration of LP–CP transformation. Different colors are for distinguishing the x and y elements, and the substrate. They are all made out of the same dielectric material.

the reflection. Most microstrip-based metallic array elements are only able to tune their geometries in two dimensions, which restricts the phase tuning capability of the unit cell. The ability of tuning the geometry in the third dimension (z-axis) not only increases the maximum phase tuning range without increasing the unit cell footage but also improves the smoothness of the phase curve. Furthermore, freely tuning in the third dimension is particularly useful for the LP–CP reflectarray design.

To achieve wideband CP wave in a unit cell design, the x and y elements are required to meet two conditions: 1) consistent $\pm 90°$ phase difference of x and y elements at all conditions (different locations, incident angles, and frequencies) and 2) stable phase response for both x and y elements across a large bandwidth. The independent control of the two orthogonal linear polarizations helps to realize consistent $\pm 90°$ phase difference. In other words, high polarization purity should be ensured when tuning the array elements' geometries. Therefore, the x and y elements are designed to have a high aspect ratio so the long edge is in the plane of its primary polarization, i.e., x element has its long edge in x-axis, the y element has the long edge in the y-axis, and the tuning in the element width should be avoided, so the y polarized wave is not affected by the tuning of x element, and vice versa. In this work, we only vary H_x and H_y but keep L_x, L_y, W_x, and W_y as constant values, so the impact on the polarization purity due to the changes in x and y dimensions is avoided. Since the x and y elements are identical cases, we have $L_x = L_y$ and $W_x = W_y$ in order to simplify the design.

The 3-D printable material PREPERM TP20755 was used for the dielectric array fabrication. A thin dielectric slab was 3-D printed and characterized using the Damaskos Model 600T open resonator. The measured relative permittivity and loss tangent are shown in Fig. 2. The retrieved relative permittivity and loss tangent values are 7.4 and 0.003, respectively, averaged over the frequency band 26 to 40 GHz. The measured dielectric properties were used for unit cell design and full-wave simulation of the reflectarray. A thin substrate using

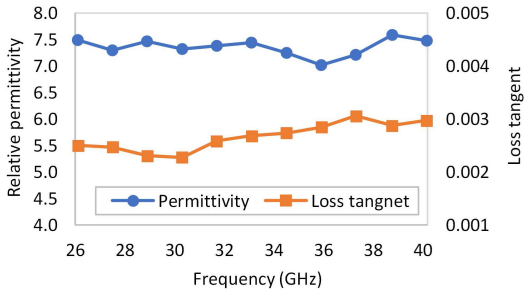

Fig. 2. Measured dielectric property of the PREPERM TP20755 material.

TABLE I
DIMENSIONS OF THE PROPOSED UNIT CELL IN MM

P	L_x	L_y	W_x	W_y	H_x	H_y	h
5	4	4	0.5	0.5	0-20	0-20	0.2

the same dielectric material with a thickness of $h = 0.2$ mm was designed to support the array elements and keep them in place during fabrication. The dimensions for the unit cell are shown in Table I. Extensive simulations were carried out to find the optimal dimensions of the unit cell that is shown in Table I. These dimensions were chosen to satisfy the manufacturing tolerances but, more importantly, to support the broadband reflectarray design. The dimensions acquisition process will be presented in Section II-B.

The unit cell is modeled using the commercial full-wave solver CST Microwave Studio with Floquet boundary conditions. Considering a unit cell with the y-element only ($H_x = 0$ mm and other parameters, as listed in Table I), the reflection phase and magnitude of the unit cell at 32 GHz for both x and y-polarized incident waves were simulated. In the ideal case, one expects large phase variation with the y-polarized wave and minimal phase variation with the x-polarized wave. In other words, the phase control of the x elements should

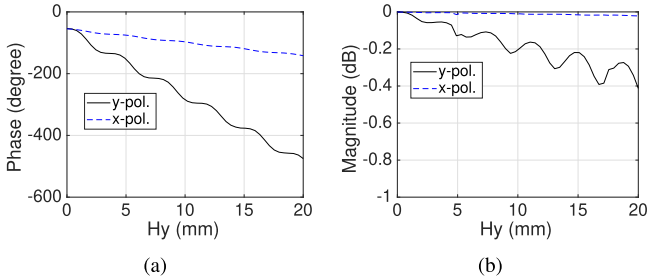

Fig. 3. Simulated reflection (a) phase and (b) magnitude with $H_x = 0$ at 32 GHz for y-polarized and x-polarized incident waves. The incident angle is 15°.

be independent of the height of the y elements nearby, and vice versa. As can be seen from Fig. 3(a), a 360° phase variation can be achieved by varying H_y from 0 to 17 mm with the y-polarized wave. By contrast, the phase variation with the x-polarized wave is considerably smaller due to the high aspect ratio of the y element. The reflection magnitude indicates how lossy the unit cell is as a reflectarray element. As shown in Fig. 3(b), the reflection loss with the y-polarized wave is above -0.4 dB for all H_y values. In comparison, the loss is almost flat and close to 0 dB for the x-polarized case, which means that the y-element alone is neglectable in the presence of x-polarized waves. The small reflection loss in both cases suggests that the proposed unit cell is a good candidate for reflectarray design at the Ka-band.

The independent tunability is verified by performing a detailed parametric study. More specifically, Ly, Wy, and Hx were investigated to evaluate their effects on the reflected phase as a function of Hy. Due to the symmetry of the structure, the characterization of Ly and Wy can be directly applied to the Lx and Wx values. Fig. 4 demonstrates the simulated phase curves at a representative frequency of 32 GHz. For simplicity, only six curves with both x- and y-polarized incident waves are plotted for each parameter. As Hy is the main variable in the parametric study, the y-polarization is considered as the main polarization and, hence, x-polarization as the second polarization. All parameters use the values in Table I except those noted in the figure.

Fig. 4(a) shows that the height of the secondary element (H_x) is trivial for the main polarization. As can be noticed, the three y-polarization curves are almost parallel, the same as the three x-polarization curves. Increasing H_x only shifts the phase curve downward, and the phase variation rate remains almost unchanged for both polarizations. It is also noticed that the phase shift range is much smaller in the primary y-polarization than it is in the secondary x-polarization due to the narrow element width in the secondary polarization.

The effects of y element's width W_y and length L_y on the polarization purity are presented in Fig. 4(b) and (c), respectively. It is clear that the phase variation rate increases while increasing either W_y or L_y in the main polarization. However, the differential of the phase curves is also increased in the second polarization with the increased W_y, as shown in Fig. 4(b). This indicates that the elements' width should be small to ensure high polarization purity.

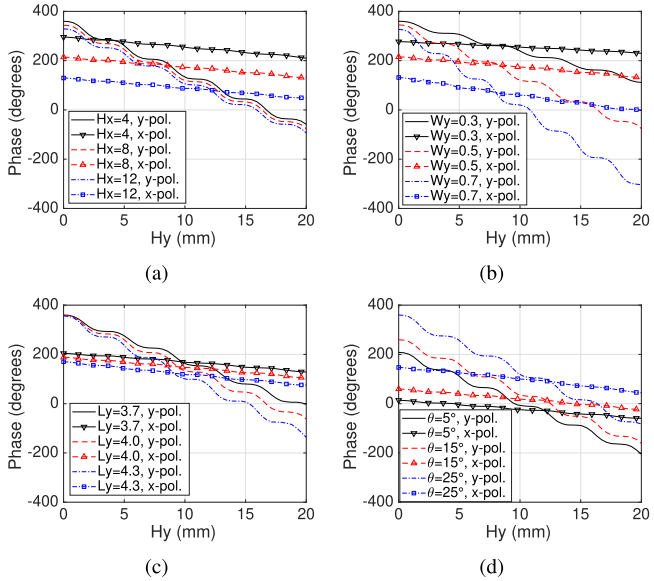

Fig. 4. Simulated reflection phase as a function of H_y while varying (a) H_x, (b) W_y, (c) L_y, and (d) θ at 32 GHz. To make comparison easier, the maximum phase is shifted to 0° for each frequency in each figure.

Since the reflectarray is designed to have an offset feed, the impact of the oblique incident angle θ is also evaluated, and the simulated phase responses are plotted in Fig. 4(d). The polarization of the incident wave remains constant and is independent of the incident angle. As can be noticed, the phase variation phase curves are almost parallel as θ is increased from 5° to 25°. This indicates neither the x nor y elements are sensitive to the incident angle of the impinging wave at the designed frequency. In practical setups, θ should be selected not to be too small, which results in feed blockage, but also not too large, which worsens the shadowing effect caused by tall elements. Moreover, the phase sensitivity at other frequency points should also be studied for broadband designs.

B. Enabling Wideband Phase Response of the Unit Cell

As mentioned in the previous section, the second condition for wideband CP waves is to have a stable phase response across a range of frequencies as wide as possible. This helps to ensure ±90° phase difference across a wideband frequency range, which results in a large AR bandwidth. Fig. 5 shows the 2-D phase maps over the frequency range from 25 to 40 GHz for different H_y values in the primary polarization. It can be noticed that, in all figures, the phase range increases as frequency increases. This is expected as the wavelength is smaller at higher frequencies. With fixed dielectric geometry, higher frequency waves travel more wavelengths and, hence, exhibit a larger phase range.

Fig. 5(a) and (b) shows the phase maps at $W_y = 0.3$ mm and $W_y = 0.7$ mm, respectively. In the first case, the phase variation from the lower end frequency to the higher end frequency and from the lower H_y to the higher H_y is very smooth, and no disruption is observed. This is a perfect example of stable phase response across the whole frequency band. However, a full 360° phase range cannot be guaranteed at lower frequencies. Only 178° phase range is

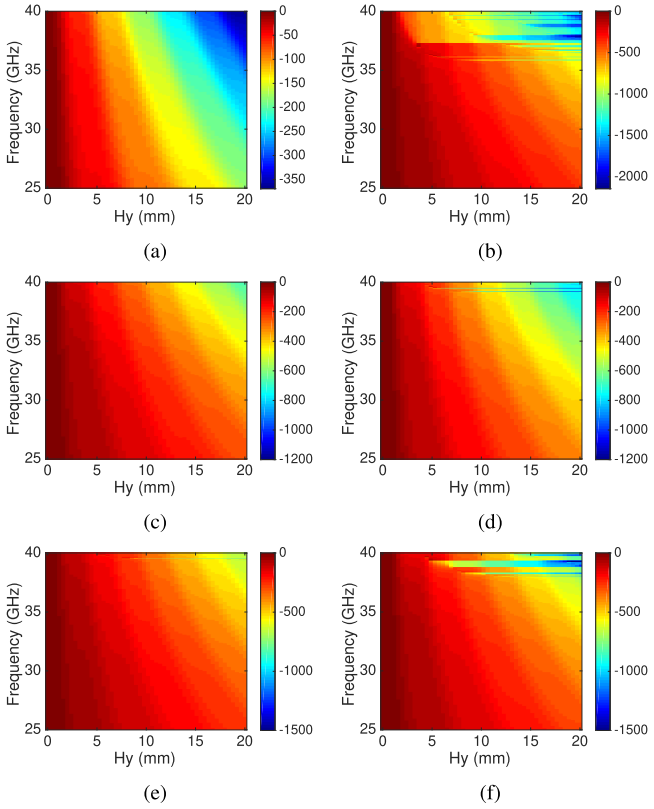

Fig. 5. Simulated reflection phase maps for different H_y and frequency values: (a) $W_y = 0.3$ mm, (b) $W_y = 0.7$ mm, (c) $L_y = 3.7$ mm, (d) $L_y = 4.3$ mm, (e) $\theta = 5°$, and (f) $\theta = 25°$ in the case of y-polarized incident wave. To make it easier for comparison, the maximum phase is shifted to 0° for each frequency in each figure.

achieved at 25 GHz. In comparison, the $W_y = 0.7$ mm case shows a larger phase range due to the increased dielectric volume. Nevertheless, it can also be noticed that the phase becomes highly sensitive to the change of element height above 36 GHz—see top right area of Fig. 5(b). This disruption will introduce large phase errors at higher frequencies, which, in turn, reduces the bandwidth of the reflectarray. In addition, too large a width also results in large phase variation in the second polarization, which should be avoided. Therefore, the element widths W_x and W_y were chosen as 0.5 mm to satisfy the minimal fabrication feature that can be reliably 3-D printed by using a 0.4 mm extruder.

The phase maps with $L_y = 3.7$ mm and $L_y = 4.3$ mm are presented in Fig. 5(c) and (d). Unsurprisingly, a larger L_y value leads to a larger phase range. Also, similar to the $W_y = 0.3$ mm case, full 360° variation at lower frequencies cannot be achieved with $L_y = 3.7$ mm. What stands out in Fig. 5(d) is its relatively stable phase response at such large values. A higher phase variation means that a smaller H_y is required to achieve a full 360° range. For 3-D printed dielectrics, it is desirable to have a smaller height for the sake of mechanical robustness. Moreover, tall elements might block electromagnetic waves from reaching the surrounding short elements. In this regard, large values of L_y and W_y are preferred. However, it should be noted too a large L_y value means that the x and y elements will physically overlap. The

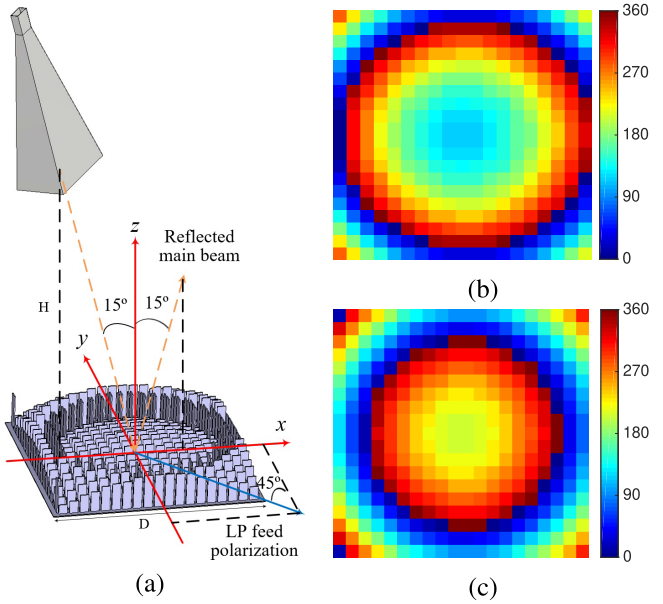

Fig. 6. Configuration of the proposed reflectarray. (a) CST model and realized phase maps of (b) x elements and (c) y elements calculated at 32 GHz.

geometry changes become insignificant when the two elements overlap, which reduces the phase tunability. Therefore, the final values of L_x and L_y are chosen to be 4.0 mm.

Finally, phase maps of incident angle of $\theta = 5°$ and $\theta = 25°$ are plotted in Fig. 5(e) and (f) using the same scale. The two figures indicate that, although not evidently, increasing the incident angle can slightly increase the phase range. However, phase disruption is also noticed in the $\theta = 25°$ case at the higher end frequency. Therefore, to minimize the phase errors but also mitigate feed blockage, the phase curve for $\theta = 15°$ was chosen for the reflectarray design.

III. Design of Ka-Band CP Reflectarray

Using the unit cell parameters determined from Section II, a CP all-dielectric reflectarray is proposed and shown in Fig. 6. The operation mechanism of a reflectarray is similar to that of a phased array antenna where array elements are individually tuned to generate required phases for beam-forming [41]. The only difference is that the phase variation from the feed to each element should be considered in the reflectarray case. Therefore, the required phase compensation for each element can be calculated by

$$\phi_i(f) = k(|\boldsymbol{r}_i - \boldsymbol{r}_f| - \hat{u}_0 \cdot \boldsymbol{r}_i) + \triangle\phi \tag{1}$$

where $\boldsymbol{r}_i$ and $\boldsymbol{r}_f$ are the position vectors of the ith element and the feed, respectively. $\hat{u}_0$ is the unit vector in the main beam direction, and $\triangle\phi$ is a constant reference phase added to all the elements. $\triangle\phi$ introduces an additional degree of freedom for the reflectarray design, which varies from 0 to 360°. The required phases for x elements are manually added with ±90° phase difference in comparison to the y elements to achieve circular polarization. The LP feed is placed in the xoz plane and tilted 15° from the broadside to mitigate feed blockage effects. By rotating the feed 45°, the LP incident wave can be decomposed into two orthogonal components in both x and y

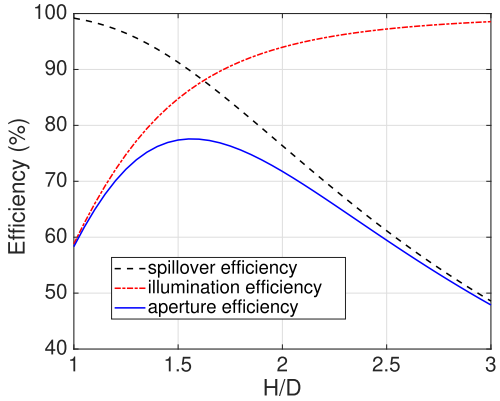

Fig. 7. Calculated aperture efficiency as a function of the ratio of feed height to aperture dimension with a 19.7 dBi horn offset by 15°.

dimensions. In addition, to minimize beam squint, the main beam direction is set to 15° off broadside in the xoz plane.

A. Optimized Aperture Efficiency

One of the most important considerations in reflectarray antenna design is aperture efficiency. This parameter indicates how efficiently the physical area of the antenna is utilized and should be maximized in the system design [41]. Aperture efficiency is defined as the product of spillover efficiency and illumination efficiency. More specifically, it is associated with parameters such as feed pattern, location and orientation, element pattern, aperture size, and shape. We aim to design a CP reflectarray that works across the entire Ka-band from 26 to 40 GHz. The aperture size is fixed at 100×100 mm^2 ($10.6\lambda \times 10.6\lambda$ at 32 GHz), where the unit cell has a side length of 5 mm. A standard gain pyramid horn antenna operating from 26 to 40 GHz was used as the feed with the gain of 19.7 dBi and a half-power beamwidth of 19° at 32 GHz. With the feed antenna, feed orientation, and aperture size determined, the aperture efficiency can be optimized by choosing an appropriate feed height where the product of spillover efficiency and illumination efficiency achieves the maximum value. The technique illustrated in [42] is adopted to calculate the spillover efficiency and illumination efficiency. To simplify the process, the feed pattern is approximately modeled by a $\cos^q(\theta)$ function with $q = 21$.

Fig. 7 presents the calculated aperture efficiency while varying the feed height. As can be observed, the maximum efficiency is achieved at H/D = 1.55, which corresponds to a height of 155 mm. It should be noted that this is only a rough estimate of the optimum height as the $\cos^q(\theta)$ function does not represent the true radiation pattern of the feed. The final height of the feed is chosen as 150 mm after comparison of simulations at a few different heights around 155 mm. With this system setup, the edge taper at the lower edge center ($x = -50, y = 0$), upper edge center ($x = 50, y = 0$), and side edge centers ($x = 0, y = \pm50$), all in mm, are -11.7, -8.6, and -11.1 dB, respectively.

B. Optimized Reference Phase

In reflectarray designs, the constant reference phase $\triangle\phi$ can be optimized to achieve the best performance [5]. This is particularly true for reflectarrays that utilize 3-D elements. More specifically, varying $\triangle\phi$ changes the required phase compensation $\phi_i(f)$ and, hence, directly affects the element heights of the 3-D array. Changing $\triangle\phi$ effectively relocates the tallest dielectric cuboids. With an oblique incidence, a large incident angle with tall array elements in unwanted regions could potentially result in a strong shadowing effect, lead to increased phase errors, and deteriorate the reflectarray performance [28]. The introduction of the orthogonal elements for CP conversion further exacerbates the situation and makes it challenging to have single optimized $\triangle\phi$ for both gain and CP bandwidths.

TABLE II
EFFECT OF REFERENCE PHASE ON REFLECTARRAY BANDWIDTH

$\triangle\phi$	3-dB gain BW in GHz (fractional BW in %)	3-dB AR BW in GHz (fractional BW in %)
0°	10.7 (31.5%)	13.4 (41.0%)
45°	10.3 (30.3%)	12.2 (38.0%)
90°	10.1 (30.4%)	11.2 (35.4%)
135°	10.8 (32.8%)	8.3 (25.9%)
180°	12.4 (38.0%)	9.7 (29.9%)
225°	12.7 (39.3%)	8.1 (23.9%)
270°	13.3 (40.2%)	6.9 (19.3%)
315°	11.2 (33.0%)	9.6 (27.7%)

Full-array simulations have been carried out to further evaluate the effect of $\triangle\phi$ on the gain and AR bandwidth. The AR is calculated from

$$AR = \frac{|E_{LHCP}| + |E_{RHCP}|}{|E_{LHCP}| - |E_{RHCP}|} \tag{2}$$

where E_{LHCP} and E_{RHCP} are the left- and right-hand circular polarized field components, respectively, and they can be derived from

$$E_{LHCP} = \frac{1}{\sqrt{2}}\left(E_\theta - jE_\phi\right) \tag{3}$$

$$E_{RHCP} = \frac{1}{\sqrt{2}}\left(E_\theta + jE_\phi\right). \tag{4}$$

Table II presents the simulated 3 dB gain bandwidth, as well as the 3 dB AR bandwidth, as $\triangle\phi$ is varied from 0° to 315° with 45° intervals. Note that the phase curve of the unit cell that is used for this calculation is normalized to start from 360°. The table shows that the highest gain bandwidth and AR bandwidth are achieved by using $\triangle\phi = 270°$ and $\triangle\phi = 0°$, respectively. The selection of different $\triangle\phi$ results in a difference of up to 9.9% in gain bandwidth—maximum fractional bandwidth of 40.2% for $\triangle\phi = 270°$ and minimum fractional bandwidth of 30.3% when $\triangle\phi$ is 45°. Different $\triangle\phi$ choices result in differences of up to 21.7% in the AR bandwidth—maximum fractional bandwidth of 41.0% when $\triangle\phi$ is 0° and minimum fractional bandwidth of 19.3% when $\triangle\phi$ is 270°. It shows that the effect due to the selection of $\triangle\phi$ is more pronounced on the AR bandwidth than on the gain bandwidth. Since, in this work, we aim to ensure good circular polarization performance over a wide bandwidth, our final choice for $\triangle\phi$ is 0°, and we proceed to calculate the

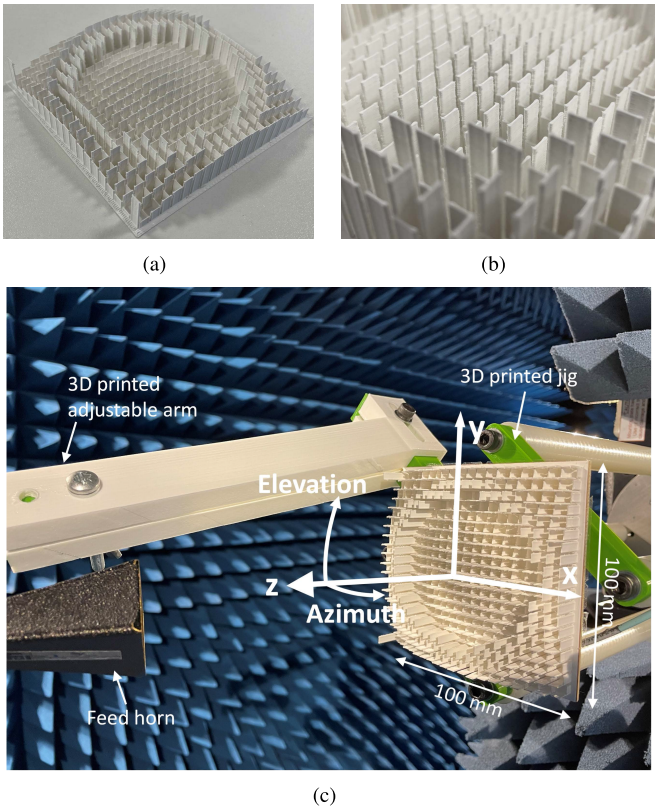

Fig. 8. Photographs of (a) printed reflectarray with (b) zoomed-in view of the x and y elements and (c) measurement setup.

required phase for each element in accordance with (1). The final achieved phase map is shown in Fig. 6(b) and (c) for both x- and y-elements.

C. Fabrication and Measurement Results

The reflectarray was 3-D printed in one single print job by using the Raise3D Pro2 with a 0.4 mm extruder. The layer height was set as 0.01 mm to ensure smooth unit cell surfaces. Before printing the entire reflectarray, the printing parameters (including the extrusion rate, extrusion overlaps, temperature, and fan speed) were optimized by printing small parts of the reflectarray and measuring the dimensions of the array elements. Then, the printing parameters were adjusted to ensure the fabricated dimensions agreed with the design dimensions. The ground plane was made of adhesive copper foil. Then, the reflectarray was affixed onto a 3-D printed jig with an adjustable extension arm, which holds the feed horn in front of the reflectarray. The adjustable arm was also 3-D printed with hollow internals that minimize their effect on the radiation pattern. The reflectarray was measured in a spherical near-field anechoic chamber. A Fast-Fourier transformation was applied to convert the near field data to the far-field. Fig. 8 shows the photograph of the fabricated reflectarray and the final setup for measuring the LP-RHCP reflectarray. The incident angle of the LP feed is set as Azimuth $= -15°$ and Elevation $= 0°$, and the reflection beam points at Azimuth $= 15°$ and Elevation $= 0°$. The LHCP reflectarray was achieved by rotating the LP feed by 90°. Alternatively, rotating the reflectarray by 90° while keeping the LP feed fixed can also achieve the desired reflected LHCP wave.

Fig. 9 plots the normalized radiation patterns, for both LHCP and RHCP, at four frequencies, namely, 27, 31, 35, and 39 GHz. Both the co-pol and x-pol patterns are plotted for the two circular polarizations, namely, RHCP and LHCP. The overall measured radiation patterns agree well with simulations although the measured x-pol level of the LHCP in the main beam direction at 31 GHz is slightly worse than that predicted by the simulation. The sidelobe levels (SLLs) are less than -15 dB, for both LHCP and RHCP, across the entire Ka-band, and the SLLs are further reduced to below -20 dB at the frequency of 31 and 35 GHz. The measured and simulated axial ratios (ARs) are shown in Fig. 10, where the 3 dB AR bandwidth almost covers the entire Ka-band. More specifically, the measured 3 dB AR bandwidths are 13.2 GHz (26.2 to 39.4 GHz) with the fractional bandwidth (FBW) of 40.2% for the LHCP and 13.3 GHz (26 to 39.3 GHz) with the FBW of 40.7% for the RHCP. Due to symmetric design in the reflectarray, the difference in the simulated AR for both LHCP and RHCP is negligible, and hence, only simulated LHCP results are displayed in Fig. 10.

Fig. 11 presents the results for the measured gain and aperture efficiency. It demonstrates that the measured results agree very well with those predicted by simulations using CST. We note that the LHCP gain levels coincide with those of the RHCP gain at most of the frequency points, demonstrating that the performance is consistent, regardless of the polarization. The maximum measured realized gain and directivity at 34 GHz were found to be 27.9 and 28.1 dBi, respectively, which corresponds to the maximum aperture efficiency of 38%, as plotted in the right axis of Fig. 11. However, it is worth noting that the simulated/measured aperture efficiency is considerably smaller than the ideal aperture efficiency shown in Fig. 7. This discrepancy can be attributed to a number of reasons. First, in the unit cell design, all elements are assumed to have the same incident angle; thus, only one phase response curve is used to determine the unit cell sizes. However, this is not the case as the feed is at a finite distance from the aperture. Large phase errors can be introduced if elements are far away from the aperture center. The wave blockage caused by the tall elements can further increase such phase errors. To alleviate this issue, one has to consider more accurate incident angles in the unit cell design, e.g., dividing the reflectarray into subregions and each subregion uses different phase response curves accordingly. Second, the $\cos^q(\theta)$ function radiation patterns for the feed horn and reflective elements, as used in the theoretical aperture efficiency calculation, are only approximations of the true patterns [41]. In this work, the difference between the theoretical $\cos^q(\theta)$ pattern ($q = 21$) and the true horn directivity pattern results in an illumination level difference of up to 4.7 dB on the array aperture. Such illumination level difference from different elements adds up and contributes to the discrepancy between theoretical and measured aperture efficiencies. Finally, the reference phase was adjusted to maximize the AR bandwidth at the cost of the maximum gain and the gain bandwidth. A similar approach

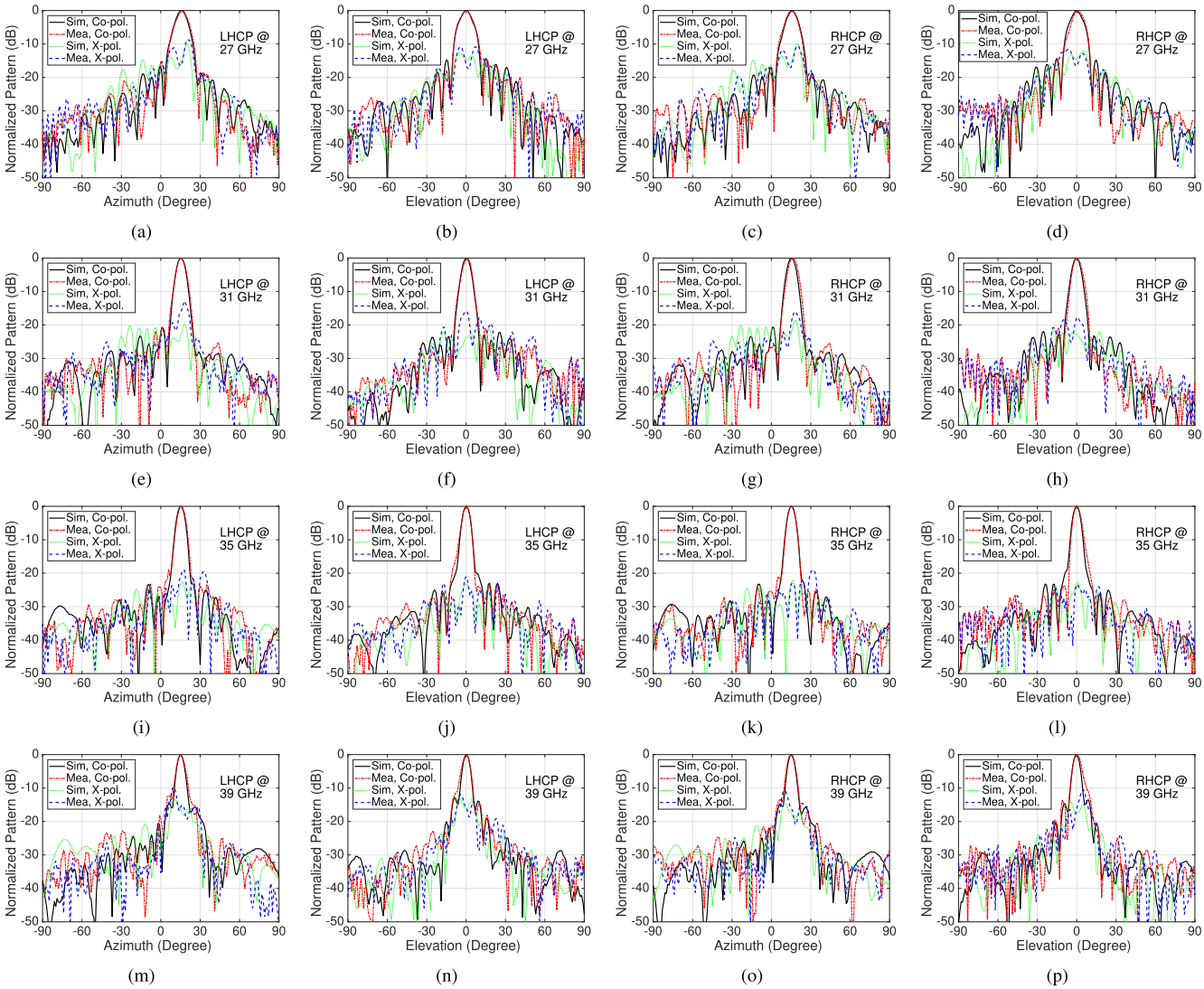

Fig. 9. Simulated and measured radiation patterns of the proposed reflectarray for both LHCP and RHCP at (a)–(d) 27, (e)–(h) 31, (i)–(l) 35, and (m)–(p) 39 GHz.

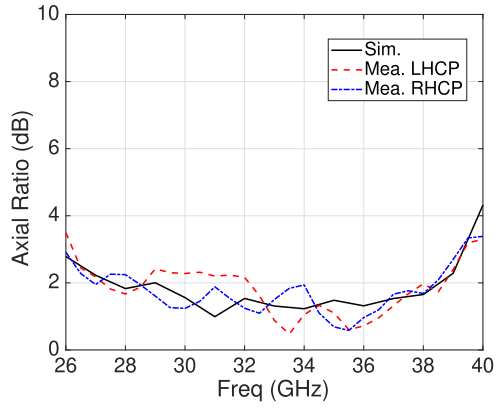

Fig. 10. Simulated and measured axial ratios for both LHCP and RHCP.

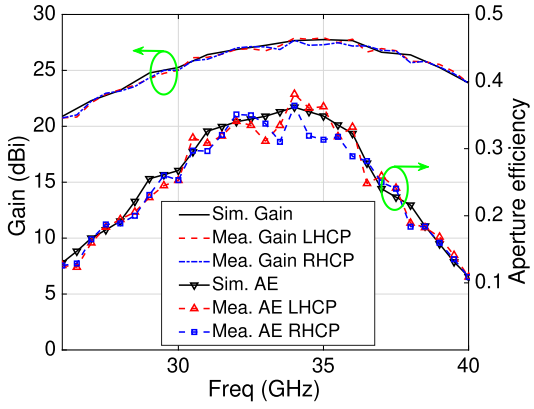

Fig. 11. Simulated and measured gain and aperture efficiency for both LHCP and RHCP.

was also reported in literature where maximum gain was reduced while optimizing the gain bandwidth [5].

The measured 3 dB gain bandwidths are 9.9 GHz (29.7–39.5 GHz) with the FBW of 28.3% for the LHCP and 10.3 GHz (29.2–39.5 GHz) with the FBW of 30.0% for the RHCP. The corresponding 1 dB gain bandwidths are 4.4 GHz (32–36.4 GHz) with the FBW of 12.9% for the LHCP and

TABLE III
COMPARISON WITH OTHER WIDEBAND CP REFLECTARRAYS

Ref.	Aperture Size	Technology	Peak Gain	Aperture Efficiency	Gain BW	3-dB AR BW
[11]	$5.4\lambda \times 5.4\lambda$	Microstrip	20.4 dBic @11.3 GHz	30%	3-dB gain 12.8%	12.5%
[12]	20λ (diameter)	Metal	31.4 dB @20.3 GHz	35%	3-dB gain 10.2%	32.5%
[31]	$5.5\lambda \times 5.5\lambda$	Dielectric	21.7 dBi @30 GHz	NaN	1-dB gain 11.2%	6.7%
[32]	$11.2\lambda \times 11.2\lambda$	Dielectric	24.2 dBi @30.5 GHz	16.5%	1-dB gain 10.7%	19.3%
[38]	$9\lambda \times 9\lambda$	Microstrip	25.8 dBi @9.8 GHz	39%	1-dB gain 17%	11%
[39]	$4.2\lambda \times 4.2\lambda$	Microstrip	19.4 dBi @9.5 GHz	44%	1-dB gain 20%	28%
[40]	$15.4\lambda \times 15.4\lambda$	Microstrip	31.6 dBi @26 GHz	40.7% (L) 46.5% (R)	3-dB gain 14.1% (L) 11.6% (R)	16.3% (L) 16.8% (R)
This work	$10.6\lambda \times 10.6\lambda$	Dielectric	27.9 dBi @34 GHz	38% (L) 34% (R)	1-dB gain 12.9% (L) 17.0% (R) 3-dB gain 28.3% (L) 30.0% (R)	40.2% (L) 40.7% (R)

5.9 GHz (31.7–37.6 GHz) with the FBW of 17.0% for the RHCP. Simulations on the reflectarray with lossless dielectric and lossy dielectric (loss tangent = 0.01) were carried out and showed that the maximum gain of the antenna was reduced by 0.53 dB due to the increased loss. As the material that was used in this work has a loss tangent of 0.003, the investigative lossy simulations demonstrated that the effect on the antenna performance due to the dielectric loss was insignificant.

Finally, before closing this section, we summarize the overall performance characteristics of the proposed design and compare it with other wideband reflectarrays listed in Table III. The comparison shows that the design presented here offers the largest AR bandwidth. In particular, in comparison to the reflectarray design in [40], which employs the microstrip element approach, this work achieves both higher gain levels and AR bandwidths, even as it uses a low cost and easy-to-fabricate technology, based on 3-D printing. In addition, in comparison to other state-of-the-art 3-D printed CP reflectarrays presented in [31] and [32], our design achieves a significantly higher aperture efficiency and AR bandwidth, spanning over nearly the entire Ka-band.

IV. CONCLUSION

This article presented a 3-D printed all-dielectric LP–CP reflectarray antenna for broadband and high-gain mm-wave communication. The novel design, described herein, realizes a broadband LP–CP transformation by adjusting the 3-D element geometries of the array. A detailed unit cell analysis has been carried out to determine the appropriate geometry to achieve a wideband phase response. The height of the feed and the reference phase have also been investigated to ensure the best wideband CP performance. Finally, a 100×100 mm^2 dual circularly polarized (dual-CP) reflectarray has been designed and fabricated. Measured results demonstrate that the reflectarray achieves a maximum gain of 27.9 dBi at 34 GHz and a maximum 3 dB AR bandwidth of 40.7%. This study shows that 3-D printing is a promising technique for realizing high-gain broadband CP reflectarray antennas. With the growing potential of the additive manufacturing process and material development, the resolution of the fabrication and the mechanical strength of materials will be improved for the 3-D printed dielectrics, which can further exploit 3-D printing in RF applications.

ACKNOWLEDGMENT

The authors thank Premix for providing the PREPERM TP20755 3-D printing filament.

REFERENCES

[1] P. Nayeri, F. Yang, and A. Z. Elsherbeni, *Reflectarray Antennas: Theory, Designs and Applications*. Hoboken, NJ, USA: Wiley, 2018.
[2] J. Shaker, M. R. Chaharmir, and J. Ethier, *Reflectarray Antennas: Analysis, Design, Fabrication, and Measurement*. Boston, MA, USA: Artech House, 2014.
[3] H. Yang *et al.*, "A 1-bit 10 × 10 reconfigurable reflectarray antenna: Design, optimization, and experiment," *IEEE Trans. Antennas Propag.*, vol. 64, no. 6, pp. 2246–2254, Jun. 2016.
[4] P. Nayeri, F. Yang, and A. Z. Elsherbeni, "Broadband reflectarray antennas using double-layer subwavelength patch elements," *IEEE Antennas Wireless Propag. Lett.*, vol. 9, pp. 1139–1142, 2010.
[5] Y. Mao, S. Xu, F. Yang, and A. Z. Elsherbeni, "A novel phase synthesis approach for wideband reflectarray design," *IEEE Trans. Antennas Propag.*, vol. 63, no. 9, pp. 4189–4193, Sep. 2015.
[6] G. Wu, Y. S. Zeng, K. F. Chan, B. J. Chen, S. W. Qu, and C. H. Chan, "High-gain filtering reflectarray antenna for millimeter-wave applications," *IEEE Trans. Antennas Propag.*, vol. 68, no. 2, pp. 805–812, Feb. 2020.
[7] X.-C. Zhu, P.-P. Zhang, Y.-X. Zhang, J.-X. Ge, and Z.-H. Gao, "A high-gain filtering antenna based on folded reflectarray antenna and polarization-sensitive frequency selective surface," *IEEE Antennas Wireless Propag. Lett.*, vol. 19, no. 8, pp. 1462–1465, Aug. 2020.
[8] L. Zhang, S. Gao, Q. Luo, W. Li, Y. He, and Q. Li, "Single-layer wideband circularly polarized high-efficiency reflectarray for satellite communications," *IEEE Trans. Antennas Propag.*, vol. 65, no. 9, pp. 4529–4538, Sep. 2017.
[9] G.-B. Wu, S.-W. Qu, S. Yang, and C. H. Chan, "Broadband, single-layer dual circularly polarized reflectarrays with linearly polarized feed," *IEEE Trans. Antennas Propag.*, vol. 64, no. 10, pp. 4235–4241, Oct. 2016.
[10] J. Yin, Q. Lou, H. Wang, Z. N. Chen, and W. Hong, "Broadband dual-polarized single-layer reflectarray antenna with independently controllable 1-bit dual beams," *IEEE Trans. Antennas Propag.*, vol. 69, no. 6, pp. 3294–3302, Jun. 2021.
[11] S. R. Lee, E. H. Lim, F. L. Lo, and W. H. Ng, "Circularly polarized elliptical microstrip patch reflectarray," *IEEE Trans. Antennas Propag.*, vol. 65, no. 8, pp. 4322–4327, Aug. 2017.
[12] K. Q. Henderson and N. Ghalichechian, "Circular-polarized metal-only reflectarray with multi-slot elements," *IEEE Trans. Antennas Propag.*, vol. 68, no. 9, pp. 6695–6703, Sep. 2020.
[13] R. Deng, Y. Mao, S. Xu, and F. Yang, "A single-layer dual-band circularly polarized reflectarray with high aperture efficiency," *IEEE Trans. Antennas Propag.*, vol. 63, no. 7, pp. 3317–3320, Jul. 2015.
[14] M. R. Chaharmir and J. Shaker, "Design of a multilayer X-/Ka-band frequency-selective surface-backed reflectarray for satellite applications," *IEEE Trans. Antennas Propag.*, vol. 63, no. 4, pp. 1255–1262, Apr. 2015.
[15] P. Nayeri, F. Yang, and A. Z. Elsherbeni, "Design of single-feed reflectarray antennas with asymmetric multiple beams using the particle swarm optimization method," *IEEE Trans. Antennas Propag.*, vol. 61, no. 9, pp. 4598–4605, Sep. 2013.
[16] M. M. Salary and H. Mosallaei, "Time-modulated conducting oxide metasurfaces for adaptive multiple access optical communication," *IEEE Trans. Antennas Propag.*, vol. 68, no. 3, pp. 1628–1642, Mar. 2020.
[17] M. E. Trampler, R. E. Lovato, and X. Gong, "Dual-resonance continuously beam-scanning X-band reflectarray antenna," *IEEE Trans. Antennas Propag.*, vol. 68, no. 8, pp. 6080–6087, Aug. 2020.
[18] G. Kong, X. Li, Q. Wang, and J. Zhang, "A wideband reconfigurable dual-branch helical reflectarray antenna for high-power microwave applications," *IEEE Trans. Antennas Propag.*, vol. 69, no. 2, pp. 825–833, Feb. 2021.

[19] Z. Chen and H. Wong, "Liquid dielectric resonator antenna with circular polarization reconfigurability," *IEEE Trans. Antennas Propag.*, vol. 66, no. 1, pp. 444–449, Jan. 2018.
[20] Z.-X. Xia, K. W. Leung, and K. Lu, "3-D-printed wideband multi-ring dielectric resonator antenna," *IEEE Antennas Wireless Propag. Lett.*, vol. 18, no. 10, pp. 2110–2114, Oct. 2019.
[21] T. Hayat, M. U. Afzal, F. Ahmed, S. Zhang, K. P. Esselle, and Y. Vardaxoglou, "Low-cost ultrawideband high-gain compact resonant cavity antenna," *IEEE Antennas Wireless Propag. Lett.*, vol. 19, no. 7, pp. 1271–1275, Jul. 2020.
[22] S. Zhang, R. K. Arya, S. Pandey, Y. Vardaxoglou, W. Whittow, and R. Mittraj, "3D-printed planar graded index lenses," *IET Microw., Antennas Propag.*, vol. 10, no. 13, pp. 1411–1419, 2016.
[23] H. Yi, S.-W. Qu, K.-B. Ng, C. H. Chan, and X. Bai, "3-D printed millimeter-wave and terahertz lenses with fixed and frequency scanned beam," *IEEE Trans. Antennas Propag.*, vol. 64, no. 2, pp. 442–449, Feb. 2016.
[24] C. Wang, J. Wu, and Y.-X. Guo, "A 3-D-printed wideband circularly polarized parallel-plate Luneburg lens antenna," *IEEE Trans. Antennas Propag.*, vol. 68, no. 6, pp. 4944–4949, Jun. 2020.
[25] H. Giddens and Y. Hao, "Multibeam graded dielectric lens antenna from multimaterial 3-D printing," *IEEE Trans. Antennas Propag.*, vol. 68, no. 9, pp. 6832–6837, Sep. 2020.
[26] A. Massaccesi *et al.*, "3D-printable dielectric transmitarray with enhanced bandwidth at millimeter-waves," *IEEE Access*, vol. 6, pp. 46407–46418, 2018.
[27] X. Liu *et al.*, "Ultrabroadband all-dielectric transmitarray designing based on genetic algorithm optimization and 3-D print technology," *IEEE Trans. Antennas Propag.*, vol. 69, no. 4, pp. 2003–2012, Apr. 2021.
[28] P. Nayeri *et al.*, "3D printed dielectric reflectarrays: Low-cost high-gain antennas at sub-millimeter waves," *IEEE Trans. Antennas Propag.*, vol. 62, no. 4, pp. 2000–2008, Apr. 2014.
[29] S. Zhang, "Three-dimensional printed millimetre wave dielectric resonator reflectarray," *IET Microw., Antennas Propag.*, vol. 11, no. 14, pp. 2005–2009, 2017.
[30] M. D. Wu *et al.*, "Design and measurement of a 220 GHz wideband 3-D printed dielectric reflectarray," *IEEE Antennas Wireless Propag. Lett.*, vol. 17, no. 11, pp. 2094–2098, Nov. 2018.
[31] X. Zhao, F. Wei, B. Li, and X. Shi, "Design of circularly polarized dielectric resonator reflectarray antenna," in *Proc. Asia–Pacific Microw. Conf. (APMC)*, Nov. 2018, pp. 1552–1554.
[32] B. Li, C. Y. Mei, and X. Lv, "A 3-D-printed wideband circularly polarized dielectric reflectarray of cross-shaped element," *IEEE Antennas Wireless Propag. Lett.*, vol. 19, no. 10, pp. 1734–1738, Oct. 2020.
[33] H. Rajagopalan and Y. Rahmat-Samii, "Dielectric and conductor loss quantification for microstrip reflectarray: Simulations and measurements," *IEEE Trans. Antennas Propag.*, vol. 56, no. 4, pp. 1192–1196, Apr. 2008.
[34] Y. Yang, W. Wang, P. Moitra, I. I. Kravchenko, D. P. Briggs, and J. Valentine, "Dielectric meta-reflectarray for broadband linear polarization conversion and optical vortex generation," *Nano Lett.*, vol. 14, no. 3, pp. 1394–1399, Feb. 2014.
[35] D. Headland *et al.*, "Dielectric resonator reflectarray as high-efficiency nonuniform terahertz metasurface," *ACS Photon.*, vol. 3, no. 6, pp. 1019–1026, 2016.
[36] M. Samsuzzaman and M. Islam, "Circularly polarized broadband printed antenna for wireless applications," *Sensors*, vol. 18, no. 12, p. 4261, Dec. 2018.
[37] W. A. Imbriale, S. S. Gao, and L. Boccia, *Space Antenna Handbook*, 1st ed. Hoboken, NJ, USA: Wiley, May 2012.
[38] G. Zhao, Y.-C. Jiao, F. Zhang, and F.-S. Zhang, "A subwavelength element for broadband circularly polarized reflectarrays," *IEEE Antennas Wireless Propag. Lett.*, vol. 9, pp. 330–333, 2010.
[39] L. S. Ren, Y. C. Jiao, F. Li, J. J. Zhao, and G. Zhao, "A dual-layer T-shaped element for broadband circularly polarized reflectarray with linearly polarized feed," *IEEE Antennas Wireless Propag. Lett.*, vol. 10, pp. 407–410, 2011.
[40] Y.-Y. Chen, Y. Ge, and T. S. Bird, "An offset reflectarray antenna for multipolarization applications," *IEEE Antennas Wireless Propag. Lett.*, vol. 15, pp. 1353–1356, 2016.
[41] C. A. Balanis, *Antenna Theory: Analysis and Design*, 4th ed. Hoboken, NJ, USA: Wiley, 2016.
[42] A. Yu, F. Yang, A. Z. Elsherbeni, J. Huang, and Y. Rahmat-Samii, "Aperture efficiency analysis of reflectarray antennas," *Microw. Opt. Technol. Lett.*, vol. 52, no. 2, pp. 364–372, Sep. 2010.

Qiao Cheng received the B.S. degree in electronic and information engineering and the M.S. degree in electromagnetic theory and microwave engineering from Xidian University, Xi'an, China, in 2010 and 2013, respectively, and the Ph.D. degree from the Queen Mary University of London, London, U.K., in 2017.

From 2018 to 2020, he was Post-Doctoral Research Assistant with the Queen Mary University of London, where he worked on the EPSRC multidisciplinary Grand Challenge: Synthesizing 3-D metamaterials for RF, microwave, and THz applications. Since 2021, he has been a Research Associate with the Electromagnetic Sensing Group, The University of Manchester, Manchester, U.K. His current research interests include radar imaging and sensing, UWB antenna, lens antenna, and metasurface design.

Yang Hao (Fellow, IEEE) received the Ph.D. degree from the Centre for Communications Research (CCR), University of Bristol, Bristol, U.K., in 1998.

From 1998 to 2000, he was a Post-Doctoral Research Fellow with the School of Electrical and Electronic Engineering, University of Birmingham, Birmingham, U.K. He is currently a Professor of antennas and electromagnetics with the Queen Mary University of London, London, U.K. He has been serving as the Management Team of the Cambridge Graphene Centre, University of Cambridge, Cambridge, U.K., since 2013. He is active in a number of areas, including computational electromagnetics, microwave meta-materials and transformation optics, antennas and radio propagation for body centric wireless networks, active antennas for millimeter/sub-millimeter applications, and photonic integrated antennas. He co-published two books, such as *Antennas and Propagation for Body-Centric Wireless Communications* and *FDTD Modeling of Metamaterials: Theory and Applications*. He has published more than 200 journal articles.

Prof. Hao is an Elected Fellow of the Royal Academy of Engineering and IET. He won the 2015 IET AF Harvey Research Prize and was a co-recipient of the BAE Chairman's Silver Award in 2014 and the Royal Society Wolfson Research Merit Award. He was the Editor-in-Chief of the IEEE ANTENNAS AND WIRELESS PROPAGATION LETTERS. He founded a new open access journal. He is also the Editor-in-Chief of *The European Physical Journal* (EPJ) *Applied Metamaterials*. He was the Board Director of Isotropic Systems Ltd., Reading, U.K., where his lens design principle was adopted and developed for SATCOM applications. He is a frequent keynote speaker for many conferences.

Jack McGhee received the master's degree in chemistry from Loughborough University, Loughborough, U.K., in 2015.

He then continued his studies at Loughborough University's Design School as part of the EPSRC grant "Sustainable manufacturing of TCO inks and thin films" into developing 2-D and 3-D printable inks using conductive metal oxides for passive electronics and sensor applications. His research included printed temperature and humidity sensors and methods for the rapid fabrication of printed metal oxide nanowires using laser-based post processing. After completion of his Ph.D., he joined the EPSRC grand challenge project SYMETA in the Wolfson School of Mechanical, Electrical and Manufacturing Engineering, Loughborough University, developing manufacturing methods for 3-D printed meta-atoms, electromagnetics, and metamaterials. Following this position, he now performs research within the Department of Chemistry and National Graphene Institute, The University of Manchester, Manchester, U.K., researching graphene-based printed electronics and sensors.

William G. Whittow (Senior Member, IEEE) received the B.Sc. degree in physics and the Ph.D. degree in computational electromagnetics from The University of Sheffield, Sheffield, U.K., in 2000 and 2004, respectively.

From 2004 to 2012, he was a Research Associate with Loughborough University, Loughborough, U.K. In 2012, he became a Lecturer in electronic materials integration with the University of Loughborough, where he became a Senior Lecturer in 2014, a Reader (Associate Professor) in 2018, and a Professor in radiofrequency materials with the Wolfson School of Mechanical, Electrical and Manufacturing Engineering. He is the Head of the Wireless Communications Research Group, Loughborough University. He is a named Investigator on EPSRC grants totaling in excess of £10m. He has authored more than 250 peer-reviewed journal and conference papers in topics related to electromagnetic materials, synthetic dielectrics, dielectric measurements, 3-D printing, wearable antennas, VHF antennas, specific absorption rate, FDTD, specific absorption rate, metamaterials, heterogeneous substrates, embroidered antennas, inkjet printing, electromagnetic compatibility, RFID tags, and phantoms and genetic algorithms.

Dr. Whittow is a Senior Fellow of the Higher Education Academy. From 2007 to 2011, he was the Coordinating Chair of the Loughborough Antennas and Propagation Conference (LAPC). He has served as an Associate Editor of *Electronics Letters* (IET) and also *IET Microwaves, Antennas & Propagation*. He serves on the technical programme committees of several IEEE international conferences. He has been asked to give more than 20 invited conference presentations; a 4-day invited workshop on bioelectromagnetics and teaches about dielectric measurements at the European School of Antennas. In 2017, he won the Women in Engineering Society (WES) Men As Allies Award and he is the inaugural male Associate Fellow of WES. More than 80 of his academic journal articles can be freely downloaded here: http://publications.lboro.ac.uk/publications/all/collated/elwgw.html.

J. (Yiannis) C. Vardaxoglou (Fellow, IEEE) received the B.Sc. degree in mathematical physics and the Ph.D. degree in electronics from the University of Kent, Canterbury, U.K., in 1982 and 1985, respectively.

He joined Loughborough University, Loughborough, U.K., as a Lecturer in 1988, was promoted to a Senior Lecturer in 1992 and to a Professor of wireless communications, a post he holds since 1998. He served as the Dean of the School of Electronic, Electrical and Systems Engineering, Loughborough University, from 2006 to 2012. He established the 32-year-old Wireless Communications Research (WiCR) Group, Loughborough University, and founded the Centre for Mobile Communications Research (CMCR). He was awarded a prestigious EPSRC's Grand Challenge £5M (FEC) Award: Synthesizing 3D metamaterials for RF, microwave and THz applications, (http://gow.epsrc.ac.uk/NGBOViewGrant.aspx?GrantRef=EP/N010493/1). He is the Director of SYMETA Research Centre (www.symeta.co.uk) funded by an EPSRC Grand Challenge Award, researching in a wide-ranging topics applicable to cutting-edge wireless communications technology. SYMETA collaborates with many internationally leading companies and universities. His current research focuses primarily on metamaterial structures, additive manufacturing (3-D printing) for RF/micro/mm wave engineering.

Dr. Vardaxoglou is a fellow of the Royal Academy of Engineers (FREng). He has served as a consultant to various industries, holds six patents and is the Founder/Technical Director of Antrum Ltd. He has attracted research funding from industry and has been awarded 20 EPSRC research grants. He has published over 400 refereed journals and conference proceeding papers (with over 8775 citations) and has written a seminal book on *Frequency Selective Surfaces* (FSS). He was the Chairman of the Executive Committee of the IET's Antennas and Propagation Professional Network in the U.K., and chaired the IEEE's Distinguish Lecturer Program of the Antennas and Propagation Society (APS) for five years. He founded the Loughborough Antennas & Propagation Conference (LAPC), which has been running since 2005. He has chaired numerous IEE/IET events and has served on the Steering Committee of the European Conference on Antennas and Propagation, EuCAP. He was the General Chair of EuCAP 2007.

Raj Mittra (Life Fellow, IEEE) is currently a Professor with the Department of Electrical and Computer Engineering, University of Central Florida (UCF), Orlando, FL, USA, where he is the Director of the Electromagnetic Communication Laboratory. He also holds an appointment at Pennsylvania State University, University Park, PA, USA. Prior to joining Penn State, he was a Professor in electrical and computer engineering at the University of Illinois in Urbana–Champaign from 1957 to 1996.

He was the past President of AP-S, and he has served as an Editor for the *Transactions of the Antennas and Propagation Society*. He is currently the Editor-in-Chief of *FERMAT*, an e-journal published by the UCF with the endorsement of the IEEE/AP Education Society. He has received numerous awards and medals from the IEEE, as well as from the AP Society. He was recently recognized for his contributions by the URSI with the Rawer Medal and the Alexander Graham Bell Award from the IEEE Foundation. He is a Principal Scientist and the President of RM Associates, a consulting company founded in 1980, which provides services to industrial and governmental organizations, both in the U.S. and abroad. A partial list of his recent publications may be found via Google Scholar Search.

Shiyu Zhang received the Ph.D. degree from Loughborough University, Loughborough, U.K., in 2014.

Following graduation, he worked as a Research Associate with Loughborough University. He is currently with the Wolfson School of Mechanical, Electrical, and Manufacturing Engineering, Loughborough University. His current research interests include engineered electromagnetic structures (metamaterials, metasurfaces, and frequency selective surfaces), antennas and RF circuit components, additive manufacturing (3-D printing), and wearable antennas and electronic systems.

Dr. Zhang received the EPSRC Doctoral Prize Research Fellowship 2015, and he was a recipient of the 1st runner up of the 2013 Loughborough Antennas and Propagation Conference (LAPC) IET Best Student Paper Award. He served as a Technical Programme Committee Member of the LAPC in 2017 and 2018.